catalysts

MDPI

Article

Heterogeneous Asymmetric Oxidation Catalysis Using Hemophore HasApf. Application in the Chemoenzymatic Deracemization of *sec*-Alcohols with Sodium Borohydride

Hiroyuki Nagaoka

Sanyo Shokuhin Co., Ltd. R & D, 555-4 Asakura, Maebashi, Gunma 371-0811, Japan; hnagaoka@sanyofoods.co.jp; Tel.: +8127-2203-471

Academic Editor: David D. Boehr
Received: 24 December 2015; Accepted: 23 February 2016; Published: 8 March 2016

Abstract: This study aims to demonstrate the coordination of oxygen regarding the hemophore HasApf expressed by *Escherichia coli* cells, which appears to create an unlikely oxygen-activating system in HasA due to the already-coordinated iron. In the asymmetric oxidation of *rac*-1-(6-methoxynaphthalen-2-yl)ethanol (*rac*-**1**) using dissolved oxygen, the signals at *g*-values of 2.8, 2.22, and 1.72 in the electron spin resonance (ESR) spectra disappeared in conjunction with the promotion of oxoferric (Fe^{III}–O–O^{-}) species in the distal site. These results suggest that the iron of porphyrin/Fe may be oxidized in water, leading to exhibition of greater asymmetric oxidation activity in the promotion of oxoferryl (Fe^{IV}=O) species. A ketone (~50% chemical yield) produced from (*R*)-(−)-*sec*-alcohol can be desymmetrized by $NaBH_4$ in aqueous medium at 40 °C (>99% enantiomer excess, *ee*, >90% chemical yield) in the absence of NAD(P). Therefore, HasA can be regenerated via successive asymmetric catalytic events through an incorporated iron electron-transfer system in the presence of oxygen: Fe^{II} + O_2 → Fe^{III}–O–O^{-} → Fe^{IV}=O (oxidizing *rac*-**1**) → Fe^{II} + H_2O. This process is similar to a Fenton reaction. The use of a HasA-catalytic system with an incorporated redox cofactor for asymmetric oxidation overcomes the apparent difficulties in working with pure dehydrogenase enzyme/redox cofactor systems for biotransformations.

Keywords: enantioselective oxidation; hemophore HasA; heterogeneous enzyme catalysis; iron electron-transfer system; iron porphyrin

1. Introduction

A review covering the well-known alcohol dehydrogenase enzyme system that incorporates redox cysteine disulfide bonds, redox zinc, and a redox cofactor has already been published [1]; moreover, the high cost and instability of the redox cofactors in enzymatic synthesis justifies efforts to regenerate them [2]. However, the use of a HasA hemophore incorporating an iron electron-transfer system for the asymmetric oxidation (with oxygen) of secondary alcohols in organic synthesis has not yet been examined as a heterogeneous enzyme catalysis reaction [3]. However, it is generally accepted that the system of hemophore HasA secreted by host ABC transporters [4] enables heme uptake across the cell outer membrane [5] and spontaneously transforms it into the HasR receptor at the heme-binding site [6]. Thus, the use of a porphyrin/Fe holoprotein (e.g., HasA) system counteracts the apparent difficulties in working with pure dehydrogenase enzymatic/redox-cofactor systems for microbial biotransformations [7]. One of the key structural features that makes cytochrome P450 a good system to activate oxygen and catalyze oxidation reactions is that its heme iron is coordinated by a cysteine ligand in the proximal site [8] and the distal site is open for oxygen binding [9]. For all structures wherein a ligand of hemophore HasA serves as a coordinating ligand, the ligand in the proximal site is

a histidine and the distal site of the heme is coordinated by a tyrosine [10]. This set of ligands appears to make the heme in HasA an unlikely oxygen-activating system because of the already-coordinated iron (Scheme 1) [11].

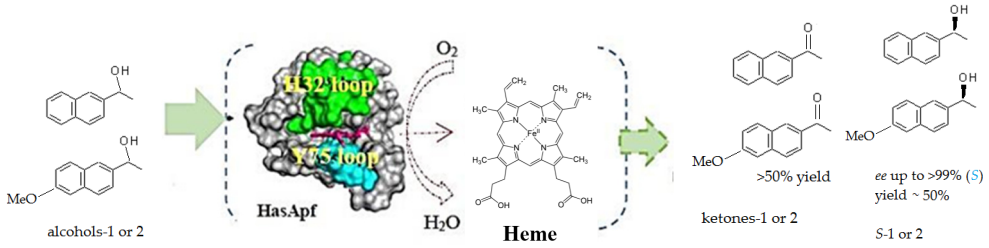

Scheme 1. The structural representation of hemophore HasA for asymmetric oxidation.

The development of deracemization methods, which yield a single stereoisomer from a racemate, is an important topic in organic synthesis [12]. The deracemization methods are classified according to the stereochemical course of enzymatic and chemical reactions [13], and special emphasis has been devoted to the theoretical background of the one-pot, single-step deracemization of *sec*-alcohols [14]. The primary feature of deracemization via bio- or chemo-catalysts or combinations thereof is its applicability to secondary alcohols [15]. An important topic in research related to such catalytic processes is the development of new biocatalysts, irrespective of whether the application of the HasA kinetic resolution to the chemoenzymatic methods involves a one-pot protocol (Scheme 2) [16].

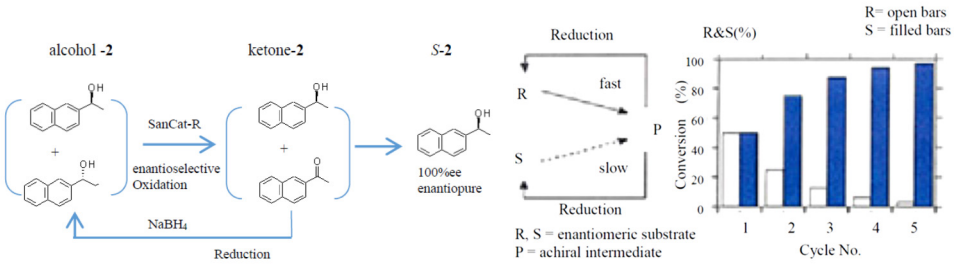

Scheme 2. Multiple oxidative kinetic resolution cycle and cyclic deracemization employing HasApf and $NaBH_4$.

Over the past decade, the use of biomaterials as plant catalytic systems incorporating redox cofactors for asymmetric oxidation reactions has been investigated [17,18]. Particularly, the redox protein eluted from pea protein (PP) encapsulated with calcium alginate gel (PP gel) is available for synthesis [19] and the enantiomeric resolution of *m*- and *p*-substituted racemic aryl methyl carbinols [20]. Specifically, membrane-bound enzymes (MEs) are activated by a buffered glycine reaction solution (pH 9.0–10.0) [21]. When eluted from encapsulated PP, under aeration, ME can be applied to turnover kinetic resolutions; e.g., MEs can be used to synthesize (*S*)-(+)-**1** ((*S*)-naproxen precursor [22]) via a polyethylene glycol (PEG) 4000-coated ME [23]. Moreover, an iron electron-transfer system can be incorporated as an oxygen-driven catalytic system for asymmetric oxidation [7]. The exact nature of the species engaged in the key reaction has been demonstrated to be consistent with that of a heme-binding protein [24]. An N-terminal sequence comparison also provides 93% similarity with a 20.853 kDa hemophore HasApf gene product (*Pseudomonas fluorescens* Pf-5) [25]. Therefore, these features are regenerated by successive asymmetric catalytic events using an incorporated iron electron-transfer system in the presence of oxygen [26]. This process is similar to that utilized by the oxygen-driven cytochrome P450: cysteine–Fe^{II} + O_2→Fe^{III}–O–O^- → Fe^{IV}=O (oxidizing *rac*-**1** or -**2**) → Fe^{II} + H_2O [7].

Two notable issues are whether oxygen can bind at a distal site because the HasA hemophore is typically coordinated by histidine (proximal) and tyrosine (distal) [27] and whether the cyclic deracemization can occur via these proteins for oxygen activation [28]. Therefore, we conducted experiments using electron spin resonance (ESR) spectroscopy and cyclic deracemization. This study aims to (1) demonstrate the coordination of oxygen by ESR evidence; (2) demonstrate the cyclic deracemization process using HasA and $NaBH_4$; and (3) present HasAs as a new asymmetric oxidation catalysis tool similar to a Fenton reaction.

2. Results and Discussion

2.1. Characterization of HasApf

2.1.1. Purifications of HasApf from PP

The purification of a HasApf from PP and the kinetic resolutions of *rac*-**2** for each fraction are summarized in Scheme 3 [21]; method details are provided in the Experimental Section. The preparation procedure was previously reported elsewhere [23], and HasApf was demonstrated to be effectively purified with a supernatant 2 sample via ultrafiltration processes using a Vivaspin molecular-weight cutoff (MWCO) 10 kDa, which is a protein sample concentrator that can surprisingly yield a single band of HasApf [23]. Table 1 and Scheme 3 also show that *P. fluorescens* Pf-5 is absent in the PP analysis for common bacteria (CFU/g), whereas aerobic spore-bearing bacteria (*Geobacillus*, *Alicyclobacillus*, *Bacillus*, *Paenibacillus*) and catalase-positive and Gram-positive cocci (*Staphylococcus*, *Kocuria*, *Micrococcus*) are detected [25]. Therefore, we speculated that the existence of the hemophore may be due to broad acquisition by the plant (e.g., PP) rather than by bacterial contamination [25].

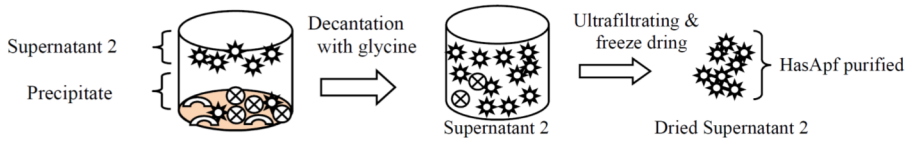

Scheme 3. Purification process of a HasApf eluted from pea protein (PP) gel under aeration.

Table 1. Relation of the amount of bacteria to the kinetic resolutions of *rac*-**2** for each fraction.

Process (each fraction)		Materials	Bacteria (CFU/g)		Resolutions			Outcomes
					rac-**2**/ catalyst	Times	Result	
1	PP[g]	powder	210[f]	Detected types: 1. aerobic spore-bearing bacterium (*Geobacillus, Alicyclobacillus, Bacillus, Paenibacillus*) 2. catalase-and gram-positive coccus bacterium (*Staphylococcus, Kocuria, Micrococcus*)				
2	PP[g] gel under aeration	Na^+alginate	ND[a]					
		$Ca^{2+}Cl_2$						
		D.W.[j]						
		PP gel	∞					
3	PP[g] gel suspension	solution			1.2 mM/5 mL[b]	10 h	N.R.[d]	HasApf weakly activated
4	Supernatant 1	solution						
5a	Precipitate 1 dried	powder	ND[a]		1.2 mM/30 mg[c]	15 h	C.R.[e]	HasApf highly activated by buffered glycine
6	Precipitate 2 dried	powder						
6a	AG[h]-Precipitate 2	powder						
6b	PEG[i]-Precipitate 2	powder						
7	Supernatant 2	solution	∞		1.2 mM/5 mL[b]	10 h		

ND[a] = not detected. 0.8 mM/5 mL[b] = solvent is detected as is. 1.2 mM/30 mg[c] = adding D.W. (5 mL). N.R.[d] = not completely resolved. C.R.[e] = completely resolved. 210[f] = in the test of Serial Analysis of Gene Expression, *P. fluorescence* PF-5 is not detected except the two types. PP[g] = Pea protein powder (PP-CS; Organo foodtech co., Ltd). AG[h] = Aggregation in a 5% (*v*/*v*) PEG (MW: 1000/4000 = 2/1). PEG[i] = polyethylene glycol. D.W.[j] = distilled water.

2.1.2. Identification of HasApf from Supernatant 2 Filtrated by Vivaspin

SDS-PAGE was performed on supernatant 2 after ultrafiltration with a Vivaspin 2 (MWCO 10 kDa) (10 μL) [21]. Precise analysis of the N-terminal amino-acid sequence (protein sequencing) of the single

band obtained via SDS-PAGE was accomplished using a PPSQ-21A protein sequencer (Shimadzu) [23]. The obtained amino-acid sequence was acquired using BLAST to identify regions of local similarity between the sequences [25]. As shown in Table 2, the amino-acid sequence (33 residues) of a single band was detected, and an N-terminal sequence comparison showed 93% similarity with HBP, a 20.853 kDa HasAp gene product (*Pseudomonas fluorescens* Pf-5, a plant commensal bacterium), and a similar E value (2×10^{-11}). This result is consistent with both the structure of the hemophore in Scheme 1 and the molecular mass in Figure 1. No **BLAST**-hit data exemplifying a hemophore HasA gene were detected from the plant for the connection between HBP (*P. fluorescens* Pf-5) and PP, as shown in Table 2; nonetheless, in the context of a highly conserved structure (Scheme 1) resulting from the broad acquisition by PP, amino acid sequence alignments involving a large number of HasA proteins from different organisms show strict conservation of the histidine residue that coordinates the heme iron in the proximal side. Consequently, the ultrafiltrated supernatant 2 enables the kinetic resolution of *rac*-**1** for asymmetric oxidation, although the oxidative reaction on HasApf appears difficult because of the lack of a cysteine ligand. The important consideration is whether oxygen can bind at the distal site to be activated if iron is already coordinated.

Table 2. Results of a BLAST query sequence analysis based on the N-terminal amino-acid sequence identified band from Supernatant 2.

Cycle No. for Supernatant 2			
N-terminal amino-acid sequence identified (33 residues)			
1.	M S X^a S I S Y S T X^b	Y A T N T V A Q Y L	X^a D W X^b A Y F G D L
30.	N H R E		
Cycle No. for YP 262445.1[c]			
Full length gene and protein sequence based on a BLAST query sequence analysis			
1.	M S I S I S Y S A T	Y G G N T V A G Y L	T D W S A Y F G D V
	atg agc att tcg atc tct tac agc gct acc	tac ggc ggt aat act gtt gcg caa tac ctg	act gac tgg tcg gcc tac ttc ggc gac gtc
30.	N H R P G E V V D G	T N T G G F N P G P	F D G T Q Y A I K S
	aac cac cgc cca ggc gaa gtg gtc gac ggc	acc aac acc ggt ggc ttc aac ccg ggc ccg	ttc gac ggc acc cag tac gcc atc aag agc
60.	T A S D A A F V A D	G N L H Y T L F S N	P S H T L W G S V D
	acc gcc agt gac gcg gcc ttc gtc gcc gac	ggc aac ctg cac tac acc ctg ttc agc aac	ccg agc cac acc ctg tgg ggc tcg gtg gac
90.	T I S L G D T L A G	G S G S N Y N L V S	Q E V S F T N L G L
	act atc tcc ctg ggc gac acc ctc gcc ggt	ggt tcg ggc agc aac tac aac ctg gtc agc	cag gaa gtc agc ttc acc aac ctg ggc ctc
120.	N S L K E E G R A G	E V H K V V Y G L M	S G D S S A L A G E
	aac agc ctg aag gaa gaa ggc cgt gca ggc	gaa gtg cac aag gtg gtc tac ggc ctg atg	agt ggc gac agc tcg gcg ctg gcc ggc gag
150.	I D A L L K A I D P	S L S V N S T F D D	L A A A G V A H V N
	atc gat gcc ctg ctc aag gcg atc gac cca	agc ctg tcg gtg aac tcc acc ttc gac gac	ctg gcc gct gct ggc gtt gct cac gtc aac
180.	P A A A A A A D V G	L V G V Q D V A Q D	W A L A A
	ccg gct gcc gca gcc gct gcc gat gtt ggc	ctg gtg ggt gtg cag gac gtg gcc cag gac	tgg gcg ctg gcc gcc

X^a: may be Cys (C) but not detected, X^b: many amino acids were detected. [c]YP 262445.1: the accession hit on the query sequence was limited between the query coverage (>93%) and E value (2e-11), a 20.853 Da. HasAp gene product [hemophore: *Pseudomonas fluorescens Pf-5*] from plant commensal bacteria, which can inhibit the rhizosphere and produce secondary metabolites that suppress soil-borne plant pathogens. Red amino acids indicate "hits" between Supernartant 2 and YP 262445.1[c]. Blue squares indicates the heme-binding site: His-32 (bearing loop), Tyr-75 (axial heme ligand), and His-83 (hydrogen ligand). Squares indicate the Cys (C) or Met (M) including sulfur.

2.2. *Preparation of HasApf Expressed by Escherichia coli Cells*

HasApf Protein Expression and Purification

The HasApf coding sequence was amplified by a polymerase chain reaction with bacterial genomic DNA (*P. fluorescens*) and cloned into pET28a (Novagen) to confirm whether oxygen could bind at the distal site. The resultant plasmids were transformed into BL21(DE3) *Escherichia coli* cells, and the transformants were cultured through continuous shaking at 30 °C in Terrific Broth to which 50 µL/mL ampicillin was added. The cells were lysed by sonication, and the HasApf proteins were purified from the supernatant using a His–Tag purification column. As shown in Figure 1, although cytochrome P450 electron-transport chains corresponding to NADPH→FAD-containing reductase → iron–sulfur complex→P450 have been reported [21], the HasApf shows a single band at approximately 21 kDa [23]; SDS-PAGE provided no preliminary evidence of iron sulfate participating in the HasApf [25].

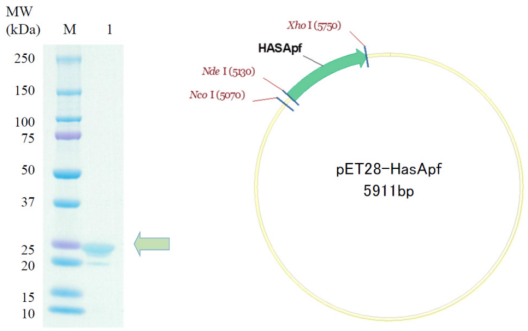

Figure 1. SDS-PAGE of a HasApf gene product (10 μL) from a cloned vector (pET28a-HASApf) which was transformed into BL21(DE3) *E. coli* cells: M = Precision Plus Protein Dual Color Standards, 1 = HasApf sample after purification. Phoresis buffer: 25 mM Tris pH 8.3, 192 mM glycine, 0.1% SDS.

2.3. Kinetic Resolution and Physicochemical Analysis

2.3.1. Asymmetric Oxidation of *rac*-**1** with Bacterial HasApf

The time course of the asymmetric oxidation activity with a HasApf expressed (40 μM: e.g., 0.36 mg) utilizing substrate *rac*-**1** (0.8 mM: e.g., 0.4 mg) in deionized water (5.0 mL) is summarized in Figure 2, where (*S*)-**1**, (*R*)-**1**, and the product ketone were monitored [21]. A redox protein obtained from expressed HasApf can oxidize an enantiomer in *rac*-**1**; thus, the other enantiomer could be obtained with high enantioselectivity (*i.e.*, 50% yield, 99% *ee*) although the activity of PP–HasApf (0.1 μM, which is equal to PEG–precipitate 2 (30 mg)) is more than 200 times greater than that of the expressed HasApf (40 μM), suggesting that a nonplanar oxoferryl (Fe^{IV}=O) species might be formed during oxidation between 0 h and 24 h incubations (Figure 2) [23]: when the iron of porphyrin/Fe of PEG–precipitate 2 and oxygen perfectly coordinates in the process of PP-gel aerations, leading to exhibition of greater asymmetric oxidation activity for the promotion of a reactive oxygen species (Scheme 3), the expressed HasApf gets coordinated to the oxygen at the distal site. Moreover, no participation of iron(II) sulfate and/or H_2O_2 in HasApf was detected, and the kinetic resolution of *rac*-**1** to (*S*)-(+)-**1** (>99% *ee*, ~50% chemical yield) via the selective oxidation of (*R*)-(−)-**1** to the corresponding ketone (Figure 2) was catalyzed [25].

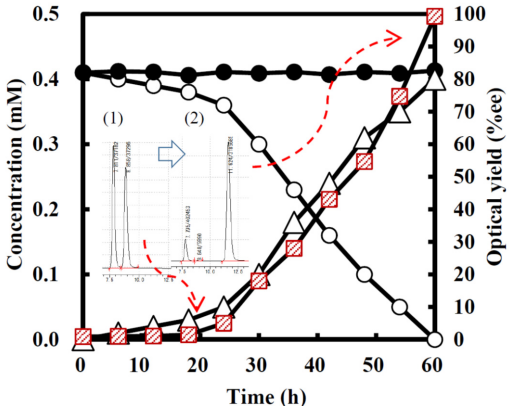

Figure 2. Time course of the asymmetric oxidation activity (-□-: % *ee*) using expressed HasApf (40 μM) and substrate *rac*-**1** (0.8 mM) in deionized water as a solvent (5.0 mL); the absorbances of (*S*)-**1** (-●-: 0.4 mM), (*R*)-**1** (-○-: 0.4 mM), and the product ketone (-△-) were monitored. Legend: A nonplanar oxoferryl (Fe^{IV}=O) species might be formed during oxidation between 0 h and 24 h incubations. Labelled arrows: 1. No oxidation activity was detected. 2. After 24 h, greater asymmetric oxidation activity was detected in the promotion of a reactive oxygen species. *There are no participation of iron(II) sulfate and/or H_2O_2 in HasApf biotransformation.

2.3.2. UV-Absorbances at Each of the HasApf Reaction Times

As shown in Figure 3, UV–vis absorption spectrophotometry (UV-3600 Plus) was performed, where the absorption at wavelengths of 410 nm (heme) and 350 nm (product ketone-2) was monitored as a function of time (0, 24, 48, and 72 h). These results indicate that, whereas the absorbance at 350 nm (product ketone) continuously increased, the absorbance at 410 nm (HasApf heme) minimally varied with reaction time. Therefore, the expressed HasApf was fairly stable in a water reaction tube without any cap at 40 °C. ESR analysis could therefore be conducted to determine whether oxygen could bind at the distal site and whether His/Tyr-heme remained in the six-coodinate low-spin state.

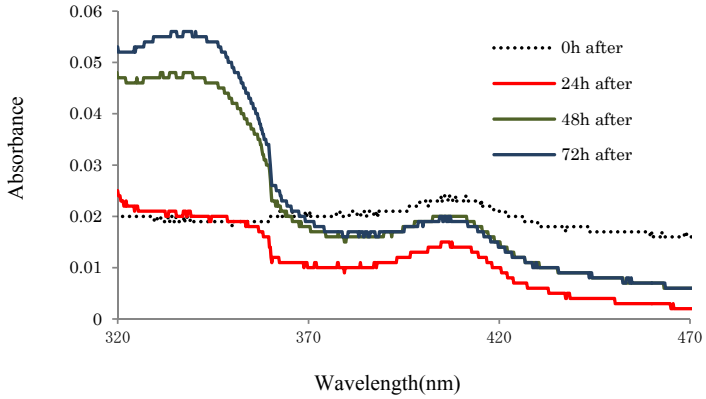

Figure 3. UV–vis absorption spectra of HasApf (40 μM)/*rac*-**2** (0.8 mM)/deionized water (5.0 mL); absorption was monitored at 410 nm (heme) and 350 nm (product ketone-2) (H) at incubation times of 0, 24, 48, and 72 h.

2.3.3. ESR Spectra at Each of the HASApf Reaction Times

As shown in Figure 4, we further confirmed whether substantial differences exist in ESR spectra related to the oxygen-binding at the distal site at each oxidative kinetic resolution time (*i.e.*, 0, 50, and 100 h). These results show that, whereas the 0 h incubation (a) may result in a six-coordinate low-spin state with His/Tyr coordinated to heme, 50 h incubation (b) appears to result in high-spin complexes with distinctive $g'_x \cong g'_y \cong 6$ and $g'_z = 2$ [27,28]; the low-spin species in the high-spin complexes, where the concentrations of low-spin species ranged from approximately 10% to 30%, generated *g*-values of $1.56 \leqslant g_x \leqslant 1.72$, $2.21 \leqslant g_y \leqslant 2.23$, and $2.78 \leqslant g_z \leqslant 2.80$ [29,30]. Furthermore, with 100 h incubation, peaks appeared at g = 4.3 and g = 2.0 in the ESR spectra of ultrafiltrated dried supernatant 2 with the promotion of oxoferryl (Fe^{IV}=O), suggesting that the iron of porphyrin/Fe may be oxidized in water to be oxoferric (Fe^{III}–O–O^{-}) species and that an oxidative iron could exhibit higher asymmetric oxidation activity in the promotion of oxoferryl (Fe^{IV}=O) species.

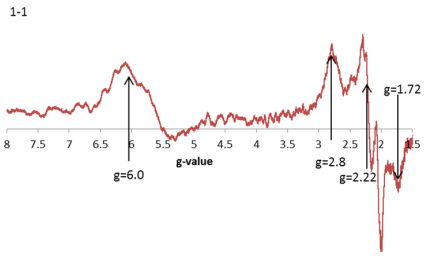

(**a**) HasApf–0 hours incubation

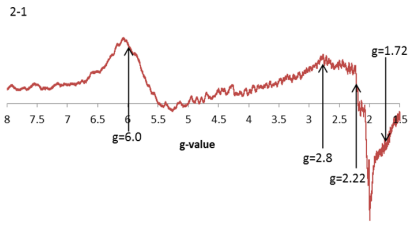

(**b**) HasApf–50 hours incubation

Figure 4. *Cont.*

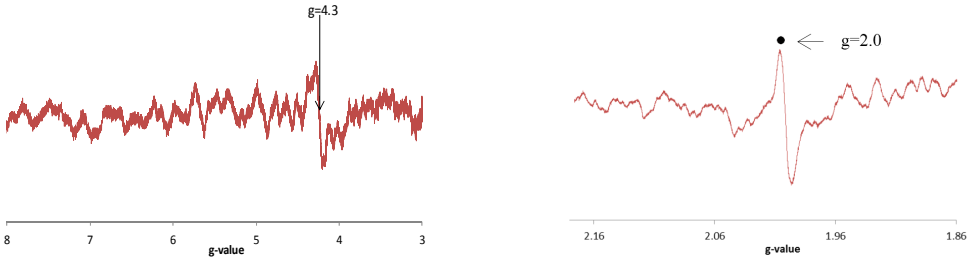

(**c**)HasApf–100 hours incubation & dried supernatant 2

Figure 4. Electron spin resonance (ESR) spectra of Fe(III) from (**a**) HasApf, 0 h; (**b**) HasApf, 50 h; and (**c**) HasApf, 100 h or ultrafiltrated supernatant 2. In (**a**), numerous signals appear at g = 6.0, 2.8, 2.22, and 1.72, suggesting the presence of axially symmetric low-spin ferric His/Tyr-heme iron; In (**b**), three signals disappear at 2.8, 2.22, and 1.72, suggesting the coordination of oxygen; In (**c**), two signals appear at g = 4.3 and 2.0, suggesting the ferric form (oxoferryl (Fe^{IV}=O)). "Signal Intensity" *y* axis appears quite noisy because of the lower concentrations of HasApf (40 μM) including *rac*-2 (0.8 mM) for ESR resolution.

2.4. Application to a Chemoenzymatic Process

Cyclic Deracemization of *rac*-**1** or -**2** Using HasApf and $NaBH_4$

After PEG–precipitate 2 (specifically, *SanCat-R*: 1.0 g) was preincubated with 400 mL deionized water at 40 °C on a rotary shaker (55 rpm) for 1 h, *rac*-**1** or -**2** (45 mg) was added to the reaction mixture; after 15 h of incubation, additional *rac*-**1** or -**2** (55 mg) was added to the mixture, which was then incubated for an additional 8 h. The substrate specificity of the PEG–precipitate 2 was investigated; the results are reported as "1st" in Table 3. The results indicate that only (*R*)-**1** or -**2** can be asymmetrically oxidized into 2-acetonaphthone (~50% chemical yield) and that (*S*)-**1** or -**2** can thereby be obtained in greater enantiomeric excess (>99% *ee*(s), ~50% yield) in the absence of NAD(P) in aqueous media at 40 °C. Afterwards, as shown in Table 3, the mixture was used for cyclic deracemization in the presence of $NaBH_4$ (50 mg × 3) in incubations conducted in 5 h intervals (2nd, 3rd, and 4th in Table 3). These results indicate that PEG–precipitate 2 (1.0 g) catalyzed only the oxidation of (*R*)-**1** or -**2** to the product ketone (~50% yield); ketone can be effectively reduced into *rac*-**1** or -**2**, thereby allowing the other enantiomer ((*S*)-**1** or -**2**: >99% *ee*) to be obtained in >90% chemical yield (ketone: <4%). Thus, the cyclic deracemization process using HasApf and $NaBH_4$ was successful.

Table 3. Application of polyethylene glycol (PEG)–precipitate 2 to the cyclic deracemization in the presence of $NaBH_4$.

Cycle No.	Deracemization: PEG–Precipitate 2 (1.0 g)/*rac*-1 (100 mg)/Deionized Water (400 mL)							
	$NaBH_4$	Time (h)	Ketone %	Alcohol % [a]	(*R*)-Isomer %	(*S*)-Isomer %	Compd	OP/%*ee* [b]
1st	0	23	49	51	1.2 1.0	98.8 99.0	(*S*)-1 [c] (*S*)-2 [d]	97.6 98.0
2nd	50 mg	28	32	68	0.8 0.7	99.2 99.3	(*S*)-1 (*S*)-2	98.4 98.6
3rd	50 mg	33	17	83	0.4 0.2	99.6 99.8	(*S*)-1 (*S*)-2	99.2 99.4
4th	50 mg	40	4	96	0.2 0.1	99.8 99.9	(*S*)-1 (*S*)-2	99.4 99.8

* Reactions: 1st: *rac*-**1** or -**2** (45 mg) → 15 h → *rac*-**1** or -**2** (55 mg) → 8 h → 2nd: $NaBH_4$ (50 mg) → 5 h → 3rd: $NaBH_4$ (50 mg) → 5 h → 4th: $NaBH_4$ (50 mg) → 7 h (total: 40 h); Note that, after *rac*-**1** or -**2** was added half (45 mg) by half (55 mg), $NaBH_4$ can be added in 5 h intervals, suggesting that a PEG–precipitate 2 asymmetric oxidation can be achieved upon the addition of $NaBH_4$; [a] Chemical yield (%); [b] enantiomer excess; [c] 1-(6-methoxynaphthalen-2-yl)ethanol; [d] 1-(2-naphthyl)ethanol.

An oxidation/hydroxylation system that includes enzymatic detoxification involving the promotion of a reactive oxygen species via an iron electron-transfer system [31] is already well known: hydroxylation [32], epoxidation [33], and dehalogenation [34] using cytochrome P450 enzyme [35] and porphyrin-like complexes [36] such as N-bridged di-iron oxo phthalocyanine [37] associating cytochrome P450 and a monooxygenase enzyme that uses H_2O_2 or mCPBA as an oxidant and NAD(P) redoxin complex [38]. Furthermore, the biological degradation of heme (iron-protoporphyrin) plays a variety of critical functions in living organisms [39]; an enzyme termed heme oxygenase (HO) has already been reported to catalyze the regiospecific conversion of heme into biliverdin, carbon monoxide (CO), and a free ferrous iron via three successive oxygenation reactions [40] (Scheme 4). The literature contains numerous reports exemplifying other types of heme degradation enzymes, e.g., the HutZ protein in the heme utilization (Hut) system [41,42] and *Mycobacterium tuberculosis* enzyme MhuD [43]. Therefore, the results in the present work newly indicate that (1) oxygen will bind at the distal site for oxygen activation to be oxoferric (Fe^{III}–O–O^-) species; (2) the iron of porphyrin/Fe and oxygen coordinates solely in water due to the promotion of oxoferryl (Fe^{IV}=O) species; (3) ESR low-spin signals (g = 2.8, 2.22, and 1.72) disappear for oxygen activation with high-spin signal contamination; and (4) HasA can be used for cyclic deracemization in combination with $NaBH_4$.

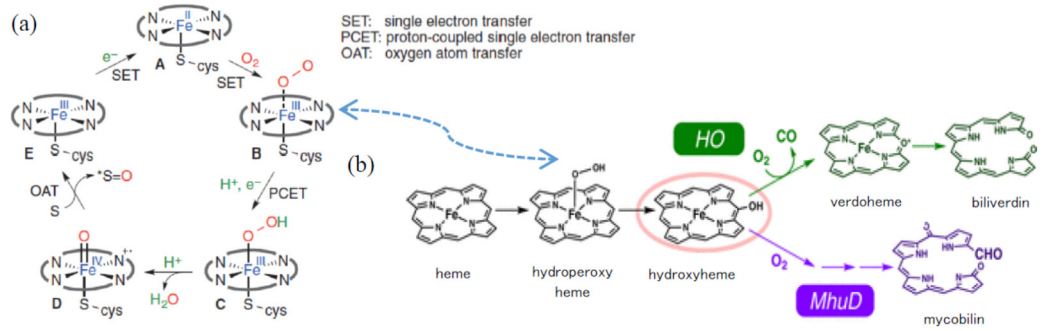

Scheme 4. (a) The incorporated iron electron-transfer system of cytochrome P-450 in the presence of oxygen: $Fe^{II} + O_2 \rightarrow Fe^{III}$–O–$O^- \rightarrow Fe^{IV}$=O (oxidizing *rac*-**1** or -**2**) $\rightarrow Fe^{II} + H_2O$. (b) The pathway of heme metabolism: either heme oxygenase enzymes (HO; E.C. 1.14.99.3; heme–hydrogen donor: oxygen oxidoreductase) catalyze the rate-limiting step in heme metabolism or MhuD catalysis does not involve verdoheme, which is the key intermediate of ring cleavage by HO.

Therefore, although further explorations of the efficiency, turnover number, or enzyme loading in comparison to other known systems for this or similar transformations are being actively pursued in this laboratory, this process would overcome the apparent difficulties in working with pure dehydrogenase enzymatic/redox-cofactor systems for biotransformation. The use of a heme-binding protein (HBP) as a HasA-catalytic system has been proposed for heterogeneous enzyme catalysis [44–46], where a redox cofactor is incorporated to perform asymmetric oxidation. In the future, bacterial HasAs are expected to become important biological catalysts for the synthesis of optically active alcohols using environmentally friendly systems that promote industrial sustainability.

3. Experimental Section

3.1. Catalyst Preparation

3.1.1. HasApf (Dried Precipitate 2) Preparation from PP(pea protein)

PP (10 g) was added to 200 mL 0.75% aqueous sodium alginate and encapsulated with $CaCl_2$ (500 mL, 39 g/L). The PP gel was air-exposed for 5 h, and the resulting HasA suspension was extracted at 40 °C with distilled water (200 mL) in a 500 mL Erlenmeyer flask through centrifugation at 150 rpm for more than 40 h. To produce AG–precipitate 2, the precipitate 1 (wet: 16 g) was

centrifuged (at 10,000 rpm for 10 min), then dissolved in a 5% (*v*/*v*) PEG (M_W: 1000/4000 = 2/1)/ 50 mM glycine–NaOH solution (pH 9.0, 100 mL) and stored for over 20 h to allow aggregation. After the storage step, the precipitate was freeze-dried under vacuum and crushed using a ball mill. PEG–precipitate 2 was prepared as follows: precipitate 1 (wet: 16 g) was dissolved in a 50 mM glycine–NaOH solution (pH 9.0, 100 mL), and PEG (M_W 4000) (500 mg) was added. Finally, to produce the dried supernatant 2, precipitate 1 (wet: 16 g) was dissolved in a 50 mM glycine–NaOH solution (pH 9.0, 100 mL) for over 3 h and the resulting mixture was centrifuged at 10,000 rpm for 10 min. The resulting supernatant 2 was ultra-filtered with the Vivaspin 2–10 K and was subsequently freeze-dried under vacuum, dried at a temperature over 50°C on a hot plate (As One: THI-1000) [−50 °C/10 Pa (1 h)→5 °C/min → +50 °C/10 Pa (22 h)], and crushed using a ball mill.

3.1.2. HasApf Protein Expression and Purification

The HasApf coding sequence was amplified by a polymerase chain reaction with bacterial genomic DNA (*P. fluorescens*) and cloned into pET28a (Novagen). The resultant plasmids were transformed into BL21(DE3) *E. coli* cells, and the transformants were cultured through continuous shaking at 30 °C in Terrific Broth containing 50 μL/mL ampicillin. At OD_{600} = 1, 0.1 mM isopropyl β-D-1-thiogalactopyranoside was added, followed by incubation at 30 °C for an additional 16 h. The harvested cells were resuspended in 15 mM potassium phosphate solution containing 1 mM EDTA and 2 mM 2-mercaptoethanol. The cells were lysed by sonication, and the HasA proteins were purified from the supernatant using a His-Tag purification column. Further purification was performed using a Sephadex G-75 gel filtration column (GE Healthcare Japan Corp., Tokyo, Japan) or a Mono Q anion-exchange column (GE Healthcare Japan Corp. Tokyo, Japan) whenever necessary. The wild-type proteins were purified to the heme-loaded holoforms.

3.1.3. SDS-PAGE of Expressed HasApf

A expressed HasApf sample (10 μL) was heated to 100 °C (5 min) after being mixed with 2 × SDS sample buffers (Sigma-Aldrich, Tokyo, Japan) and electrophoresed with a molecular marker (Bio-Rad, Tokyo, Japan) in a buffer (Tris–HCl (25 mM) and glycine (0.91 M), 0.1% SDS, pH 8.3) using an SDS-PAGE mini-system (TEFCO). After completion, the gel was stained with CBB (PhastGel Blue R, Amersham Bioscience, Tokyo, Japan).

3.1.4. General Procedure for Reactions Using (1) Expressed HasApf or (2) PEG-Precipitate 2

Rac-**1** or *rac*-**2** (1000 mg) was dissolved in 2-propanol as a cosolvent (5.0 mL, 20,000 ppm). (1) The substrate solution (20 μL, 0.8 mM) and expressed HasApf (40 μM) were combined in an 18 mm × 15 mL test tube, and the reactions were performed in deionized water (5.0 mL) at 40 °C under magnetic stirring at 700 rpm; (2) The substrate solution (0.5 mL, 20,000 ppm) and PEG-Precipitate2 (1000 mg) were combined in an Erlenmeyer flask (500 mL) to which deionized water (400 mL) was added, and the reactions were performed at 40 °C under magnetic stirring at 700 rpm. Subsequently, the reaction mixture was centrifuged at 3500 rpm (5 min) and then extracted with *n*-hexane (4.0 mL). The *ee* was calculated for *rac*-**1** or -**2** (0.8 mM or 1.2 mM), which were separated using a Daicel Chiralcel OB-H column ((S)-isomer/(R)-isomer/product ketone = 7.8/8.8/11.6 min) or a Daicel Chiralpak AS-H column ((R)-isomer/(S)-isomer/product ketone = 7.5/8.25/9.5 min) connected to a HPLC LC-10A system (Shimadzu). The analytical conditions were as follows: mobile phase, *n*-hexane/IPA: 9/1, flow rate: 1.0 mL/min, temperature: 30 °C, wavelength: UV 254 nm. The stereochemistry of the isolated optically active alcohol was identified, as reported in previous studies by comparing the specific rotation values (+ or −) obtained using a polarimeter.

3.1.5. ESR Analyses and UV–vis Spectroscopy of Expressed HasApf

ESR analysis of expressed HasA dried on a hotplate was performed using a JES-FA200 ESR spectrometer (Japan Electron Optics Laboratory Co., Ltd., Tokyo, Japan) operated under a magnetic

field of 322.5 ± 250 mT, a modulation field of 0.6 mT, a time constant of 0.3 s, microwave power of 1 mW, a sweep time of 8 min, and a temperature of −165 °C. The conversion of heme to biliverdin via asymmetric oxidation in the presence of expressed HasApf (40 μM) was measured by ESR analysis (JES-FA200, Tokyo, Japan) and UV–vis spectroscopy (UV-3600 Plus, Shimadzu Co., Ltd., kyoto, Japan) in substrate solution (20 μL, 0.8 mM). Spectra were collected at 24 h intervals after the addition of substrate solution (20 μL, 0.8 mM) to the expressed HasApf. The UV–vis spectra of the heme degradation solutions were collected at 0, 24, 48, and 72 h.

4. Conclusions

HasApf displays asymmetric oxidation activity and is capable of multiple oxidative kinetic resolution cycles of cyclic deracemization in conjunction with $NaBH_4$ additions; therefore, the signals at *g*-values of 2.8, 2.22, and 1.72 in the ESR spectra disappeared in conjunction with the promotion of oxoferric (Fe^{III}−O–O^-) species in the distal site, suggesting that the iron of porphyrin/Fe is oxidized in water, leading to exhibition of greater asymmetric oxidation activity for the promotion of oxoferryl (Fe^{IV}=O) species. The *rac*-**1** or -**2** catalyzed the kinetic resolution of (*S*)-(+)-**1** or -**2** (>99% *ee*, ~50% chemical yield) via the selective oxidation of (*R*)-(−)-**1** or -**2** to the corresponding ketone. The ketone produced (~50% chemical yield) from (*R*)-(−)-**1** or -**2** was deracemized by $NaBH_4$ (50 mg × 3) and obtained as a pure enantiomer or deracemized into a mixture in which one enantiomer was present in excess >99% *ee* (~90% chemical yield) in the absence of an added cofactor (e.g., NAD(P)) in aqueous media at 40 °C under magnetic stirring at 700 rpm. Therefore, HasApf was regenerated via successive asymmetric catalytic events using an incorporated iron electron-transfer system in the presence of oxygen: Fe^{II} + O_2 → Fe^{III}−O–O^- → Fe^{IV}=O (oxidizing *rac*-**1** or -**2**) → Fe^{II} + H_2O. This process is similar to a Fenton reaction. The use of a HasA-catalytic system with an incorporated redox cofactor for asymmetric oxidation overcomes the apparent difficulties in working with pure dehydrogenase enzyme/redox cofactor systems for biotransformation.

Acknowledgments: The author would like to thank General Manager Saburo Konoeda and Hironari Miyazato from Nagaoka Perfumery Co., Ltd. for their valuable advice. Thanks are also due to General Manager Koh Ueda from Wako Pure Chemical Industries, Ltd., for placing SanCat-*R* on the market (PEG precipitate 2: Catalog No. 351-34213 (5 g)). This study was fully funded by Sanyo Shokuhin Co., Ltd.

Conflicts of Interest: The author declares no conflict of interest.

References and Notes

1. Auld, D.S.; Bergman, T. The role of zinc for alcohol dehydrogenase structure and function. *Cell Mol. Life Sci.* **2008**, *65*, 3961–3970. [CrossRef] [PubMed]
2. Sobolov, B.S.; Leonida, D.M.; Malik, B.A.; Voivodov, I.K.; McKinney, F.; Kim, J.; Fry, J.J. Cross-linked LDH crystals for lactate synthesis coupled to electroenzymatic regeneration of NADH. *J. Org. Chem.* **1996**, *61*, 2125–2128. [CrossRef]
3. Liou, Y.; Charoenkwan, P.; Srinivasulu, Y.S.; Vasylenko, T.; Lai, S.; Lee, H.; Chen, Y.; Huang, H.; Ho, S. SCMHBP: Prediction and analysis of heme binding proteins using propensity scores of dipeptides. *BMC Bioinform.* **2014**, *15*, S4. [CrossRef] [PubMed]
4. Ozaki, S.; Nakahara, A.; Sato, T. Mechanism of Heme Uptake by Heme Acquisition System A. *Chem. Lett.* **2011**, *40*, 362–363. [CrossRef]
5. Ozaki, S.; Sato, A.; Migita, T.C.; Uchida, T.; Ishimori, K. Spectroscopic Studies on HasA from Yersinia pseudotuberculosis. *J. Inorg. Biochem.* **2014**, *138*, 31–38. [CrossRef] [PubMed]
6. Krieg, S.; Huché, F.; Diederichs, K.; Izadi-Pruneyre, N.; Lecroisey, A.; Wandersman, P.C. Heme uptake across the outer membrane as revealed by crystal structures of the receptor-hemophore complex. *Proc. Natl. Acad. Sci. USA* **2009**, *106*, 1045–1050. [CrossRef] [PubMed]
7. Shoji, O.; Fujishiro, T.; Nakajima, H.; Kim, M.; Nagano, S.; Shiro, Y.; Watanabe, Y. Hydrogen Peroxide Dependent Monooxygenations by Tricking the Substrate Recognition of Cytochrome $P450_{BS\beta}$. *Angew. Chem. Int. Ed.* **2007**, *46*, 3656–3659. [CrossRef] [PubMed]

8. Ortiz de Montellano, P.R. *Cytochrome P450: Structure, Mechanism, and Biochemistry*, 3rd ed.; Kluwer Academic/Plenum: New York, NY, USA; Boston, MA, USA; Dorcrecht, The Netherlands; London, UK; Mosow, Russia, 2004.
9. Machii, K.; Watanabe, Y. Acylperoxo-Iron (III) porphyrin complexes: A new entry of potent oxidants for the alkene epoxidation. *J. Am. Chem. Soc.* **1995**, *117*, 6691–6697. [CrossRef]
10. Jepkorir, G.; Rodríguez, J.C.; Rui, H.; Im, W.; Lovell, S.; Battaile, K.P.; Alontaga, A.Y.; Yukl, E.T.; Moënne-Loccoz, P.; Rivera, M. Structural, NMR Spectroscopic, and Computational Investigation of Hemin Loading in the Hemophore HasAp from *Pseudomonas aeruginosa*. *Am. Chem. Soc.* **2010**, *132*, 9857–9872. [CrossRef] [PubMed]
11. Giles, M.N.; Watts, B.A.; Giles, M.N.; Watts, B.A.; Giles, I.G.; Fry, H.F.; Littlechild, A.J.; Jacob, C. Metal and redox modulation of cysteine protein function. *Chem. Biol.* **2003**, *10*, 677–693. [CrossRef]
12. Steinreiber, J.; Faber, K.; Griengl, H. De-racemization of enantiomers *versus* de-epimerization of diastereomers—Classification of dynamic kinetic asymmetric transformations (DYKAT). *Chem. Eur. J.* **2008**, *14*, 8060–8072. [CrossRef] [PubMed]
13. Turner, N.J. Deracemisation methods. *Curr. Opin. Chem. Biol.* **2010**, *14*, 115–121. [CrossRef] [PubMed]
14. Hein, J.E.; Hyunh, C.B.; Viedma, C.; Kellogg, R.M.; Blackmond, D.G. Pasteur's tweezers revisited: On the mechanism of attrition-enhanced deracemization and resolution of chiral conglomerate solids. *J. Am. Chem. Soc.* **2012**, *134*, 12629–12636. [CrossRef] [PubMed]
15. Carnell, A.J. Stereoinversions using microbial redox-reactions. *Adv. Biochem. Eng./Biotechnol.* **1999**, *63*, 57–72.
16. Schober, M.; Toesch, M.; Knaus, T.; Strohmeier, G.A.; van Loo, B.; Fuchs, M.; Hollfelder, F.; Macheroux, P.; Faber, K. One-Pot Deracemization of *sec*-Alcohols: Enantioconvergent Enzymatic Hydrolysis of Alkyl Sulfates Using Stereocomplementary Sulfatases. *Angew. Chem. Int. Ed. Engl.* **2013**, *52*, 3277–3279. [CrossRef] [PubMed]
17. Nagaoka, H. Chiral Resolution Function with Immobilized Food Proteins. *Biotechnol. Prog.* **2003**, *19*, 1149–1155. [CrossRef] [PubMed]
18. Nagaoka, H. Ability of different biomaterials to enantioselectively catalyze oxidation and reduction reactions. *Biotechnol. Prog.* **2004**, *20*, 128–133. [CrossRef] [PubMed]
19. Nagaoka, H. Treatment of germinated wheat to increase level of GABA and IP_6 catalyzed by endogeneous enzymes. *Biotechnol. Prog.* **2005**, *21*, 405–410. [CrossRef] [PubMed]
20. Nagaoka, H.; Udagawa, K.; Kirimura, K. Cross-linked protein complex exhibiting asymmetric oxidation activities in the absence of added cofactor. *Biotechnol. Prog.* **2012**, *28*, 953–961. [CrossRef] [PubMed]
21. Nagaoka, H. The application of a cytochrome P450 enzyme eluted from encapsulated for the catalysis of enantioselective oxidation. *RSC Adv.* **2014**, *4*, 16333–16344. [CrossRef]
22. Thakur, V.V.; Sudalai, A. Enantioselective synthesis of (*S*)-α-arylpropionic acids via Pd-catalyzed kinetic resolution of benzylic alcohols. *Indian J. Chem. Sect. B* **2005**, *44B*, 557–561. [CrossRef]
23. Nagaoka, H. Application of a Heme-Binding Protein Eluted from Encapsulated Biomaterials to the Catalysis of Enantioselective Oxidation. *ACS Catal.* **2014**, *4*, 553–565. [CrossRef]
24. Paulsen, I.T.; Press, C.M.; Ravel, J.; Kobayashi, D.Y.; Myers, G.S.; Mavrodi, D.V.; DeBoy, R.T.; Seshadri, R.; Ren, Q.; Madupu, R.; *et al*. Complete genome sequence of the plant commensal *Pseudomonas fluorescens* Pf-5. *Nat. Biotechnol.* **2005**, *23*, 873–878. [CrossRef] [PubMed]
25. Nagaoka, H. An HASApf-Redoxin Complex causing Asymmetric Catalytic Oxidation via the Regenerative Formation of a Reactive Oxygen Species. *Dalton Trans.* **2015**, *44*, 13384–13393. [CrossRef] [PubMed]
26. Du, J.F.; Li, W.; Li, L.; Wen, G.B.; Lin, Y.W.; Tan, X. Regulating the Coodination State of a Heme Protein by a Designed Distal Hydrogen-Bonding Network. *ChemistryOpen* **2015**, *4*, 97–101. [CrossRef] [PubMed]
27. Zhou, Y.; Bowler, B.E.; Lynch, K.; Eaton, S.S.; Eaton, G.R. Interspin Distances in Spin-Labeled Metmyoglobin Variants Determine by Saturation Recovery EPR. *Biophys. J.* **2000**, *79*, 1039–1052. [CrossRef]
28. Gruber, C.C.; Lavandera, I.; Faber, K.; Kroutil, W. From a Racemate to a Single Enantiomer: Deracemization by Stereoinv-ersion. *Adv. Synth. Catal.* **2006**, *348*, 1789–1805. [CrossRef]
29. Hori, H. Analysis of the principal g-tensors in single crystals of ferrimyoglobin complexes. *Biochim. Biophys. Acta* **1971**, *251*, 227–235. [CrossRef]
30. Bizzari, A.R.; Cannistraro, S. Solvent modulation of the structural heterogeneity in iron(III) myoglobin samples: A low temperature EPR investigation. *Eur. Biophys. J.* **1993**, *22*, 259–267.

31. Lee, D.S.; Yamada, H.; Sugimoto, H.; Matsunaga, I.; Ogura, H.; Ichihara, K.; Adachi, S.; Park, S.Y.; Shiro, Y. Substrate recognition and molecular mechanism of fatty acid hydroxylation by cytochrome P450 from Bacillus subtilis. Crystallographic, spectroscopic, and mutational studies. *J. Biol. Chem.* **2003**, *278*, 9761–9767. [CrossRef] [PubMed]
32. Yosca, T.H.; Rittle, J.; Krest, C.M.; Onderko, E.L.; Beham, A.R.K.; Green, M.T. Iron(IV)hydroxide pK_a and the Role of Thiolate Ligation in C–H Bond Activation by Cytochrome P450. *Science* **2013**, *342*, 825–829. [CrossRef] [PubMed]
33. Onoda, H.; Shoji, O.; Watanabe, Y. Acetate anion-triggered peroxygenation of non-native substrates by wild-type cytochrome P450s. *Dalton Trans.* **2015**, *44*, 15316–15323. [CrossRef] [PubMed]
34. Prage, B.E.; Pawelzik, S.-C.; Busenlehner, S.L.; Kim, K.; Morgenstern, R.; Jakobsson, P.-J.; Armstrong, R.N. Location of Inhibitor Binding Sites in the Human Inducible Prostaglandin E Synthase, MPGES1. *Biochemistry* **2011**, *50*, 7684–7693. [CrossRef] [PubMed]
35. Johansson, A.-L.; Carlsson, J.; Hogbom, M.; Hosler, J.P.; Gennis, R.B.; Brzezinski, P. Proton Uptake and pK_a Changes in the Uncoupled Asn139Cys Variant of Cytochrome *c* Oxidase. *Biochemistry* **2013**, *52*, 827–836. [CrossRef] [PubMed]
36. Oldham, M.L.; Khare, D.; Quiocho, F.A.; Davidson, A.L.; Chen, J. Crystal structure of a catalytic intermediate of the maltose transporter. *Nature* **2007**, *450*, 515–521. [CrossRef] [PubMed]
37. Ratliff, M.; Zhu, W.; Deshmukh, R.; Wilks, A.; Stojiljkovic, I. Homologues of Neisserial Heme Oxygenase in Gram-Negative Bacteria: Degradiation of Heme by the Product of the*piaA* Gene of *Pseudomonas aeruginosa*. *J. Bacteriol.* **2001**, *183*, 6394–6403. [CrossRef] [PubMed]
38. McDonald, A.R.; Bukowski, M.R.; Farquhar, E.R.; Jackson, T.A.; Koehntop, K.D.; Seo, M.S.; De Hont, R.F.; Stubna, A.; Halfen, J.A.; Muonck, E.; *et al*. Sulfur *versus* Iron Oxidation in an Iron-Thiolate Model Complex. *J. Am. Chem. Soc.* **2010**, *132*, 17118–17129. [CrossRef] [PubMed]
39. Unno, M.; Ardèvol, A.; Rovira, C.; Ikeda-Saito, M. Structures of the Substrate-Free and the Product-Bound Forms of HmuO, a Heme Oxygenase from *Corynebacterium diphtheriae*: X-ray crystallography and molecular dynamics investigation. *J. Biol. Chem.* **2013**, *288*, 34443–34458. [CrossRef] [PubMed]
40. Matsui, T.; Nambu, S.; Ono, Y.; Goulding, C.W.; Tsumoto, K.; Ikeda, M. Heme degradation by *Staphylococcus aureus* IsdG and IsdI liberates formaldehyde rather than carbon monoxide. *Biochemistry* **2013**, *52*, 3025–3027. [CrossRef] [PubMed]
41. Ishimori, K.; Watanabe, Y. Unique Heme Environmental Structures in Heme-regulated Proteins Using Heme as the Signaling Molecule. *Chem. Lett.* **2014**, *43*, 1680–1689. [CrossRef]
42. Uchida, T.; Sekine, Y.; Ikeda-Saito, M.; Ishimori, K. A heme degradation enzyme, HutZ, from Vibrio cholerae. *Chem. Commun.* **2012**, *48*, 6741–6743. [CrossRef] [PubMed]
43. Nambu, S.; Matsui, T.; Celia, W.; Goulding, C.W.; Takahashi, S.; Ikeda-Saito, M. A new way to degrade heme: The *Mycobacteriaum tuberoculosis* enzyme MhuD catalyzes heme degradation without generating CO. *J. Biol. Chem.* **2013**, *288*, 10101–10109. [CrossRef] [PubMed]
44. Lam, M.K.; Lee, K.T.; Mohamed, A.R. Homogeneous, heterogeneous and enzymatic catalysis for transesterification of high free fatty acid oil (waste cooking oil) to biodiesel: A review. *Biotechnol. Adv.* **2010**, *28*, 500–518. [CrossRef] [PubMed]
45. Zhao, Z.Y.; Liu, J.; Hahn, M.; Qiao, S.; Middelberg, A.P.J.; He, L. Encapsulation of lipase in mesoporous silica yolk–shell spheres with enhanced enzyme stability. *RSC Adv.* **2013**, *3*, 22008–22013. [CrossRef]
46. Protein Sequence Based on a BLAST Query Sequence Analysis of Cycle No. for YP 262445.1 is Available on the Internet on NCBI resource: http://www.ncbi.nlm.nih.gov/protein/70732682 (accessed on 17 December 2015).